Sulfide Film Formation on Copper Under Electrochemical and Natural Corrosion Conditions

J. Smith,[‡,] Z. Qin,[*] F. King,[**] L. Werme,[***] and D.W. Shoesmith[*]*

ABSTRACT

The mechanism and kinetics of Cu corrosion in anoxic aqueous chloride solutions containing sulfide (10^{-3} mol/L) have been investigated electrochemically and under natural corrosion conditions. Under these conditions Cu is thermodynamically unstable in anoxic water, and the anodic growth of a chalcocite (Cu_2S)/digenite ($Cu_{1.8}S$) film is supported by the cathodic reduction of water. Electrochemical experiments at rotating disc electrodes and impedance spectroscopy show that the film growth occurs under SH^- transport control as stagnant conditions are approached. At this concentration, film growth can follow two distinct pathways. The initially formed film grows rapidly via an ion (or associated defect) transport process. If this film remains coherent, subsequent film growth/corrosion is extremely slow. If the development of interfacial stresses leads to film fracture, then growth continues and a much thicker nodular deposit is formed. The primary goal of this research is to develop a mixed potential model, which can be used to assess the performance of copper nuclear waste containers in granitic nuclear waste repositories.

KEY WORDS: copper, corrosion potential, electrochemical impedance spectroscopy, high-level waste, mechanism, sulfide, voltammetry

INTRODUCTION

A proposed method of disposal of Swedish/Finnish/Canadian high-level nuclear waste is to place it in corrosion-resistant containers and bury it approximately 500 m to 1,000 m deep in granite environments.[1-3] It is proposed that the waste canisters will be buried in bore holes and the excavated space between the container and the vault walls backfilled with compacted bentonite clay. The shafts and tunnels would then be backfilled with a mixture of bentonite clay and crushed granite. The primary candidate for the fabrication of these containers is copper, selected primarily because of its good thermodynamic stability in the aqueous anoxic environments anticipated in such repositories.[4] The design of these containers has been discussed elsewhere.[4] The key feature for present purposes is the proposed use of an outer copper shell (approximately 5 cm thick) and an inner liner of nodular cast iron (Figure 1).[3,5-6]

A model based on mixed potential principles has been developed to predict container lifetimes under the anoxic conditions anticipated in these locations. This model[7] shows that corrosion during the early lifetime of the vault, when significant O_2 concentrations exist, should be minimal. The mean predicted corrosion rate over the first year is ~0.3 μm/y. This low rate can be attributed to the consumption of O_2 trapped in the buffer and backfill by reaction with Fe(II) minerals and organic material, as well as to the diffusion of O_2 out of the repository. Only 17% of atmospheric O_2 trapped initially within the vault is available for reaction with the canister surface,[7]

Submitted for publication February 2006; in revised form, June 2006.

‡ Corresponding author. E-mail: jsmith6@uwo.ca.
* Department of Chemistry, The University of Western Ontario, London, ON, Canada, N6A 5B7.
** Integrity Corrosion Consulting Ltd., 6732 Silverview Drive NW, Calgary, AB, Canada, T3B 3K8.
*** SKB Swedish Nuclear Fuel and Waste Management Co., Box 5864, SE-102 40, Stockholm, Sweden.

0010-9312/07/000015/$5.00+$0.50/0

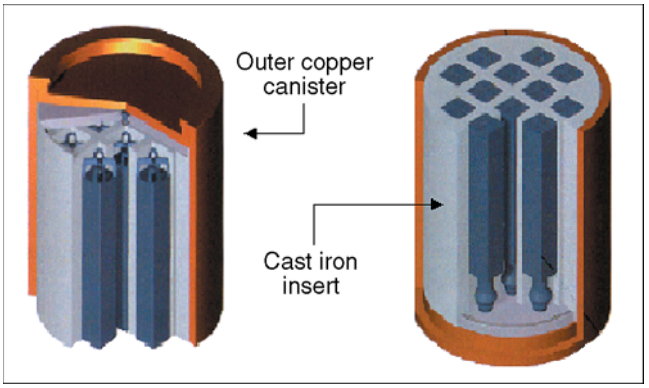

FIGURE 1. *Schematic of the proposed Scandinavian nuclear waste disposal canister composed of a corrosion-resistant copper outer layer and a carbon-steel inner liner.*

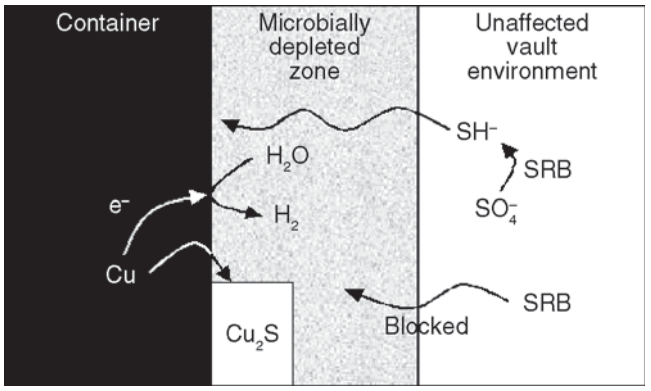

FIGURE 2. *Schematic illustrating a possible scenario for copper corrosion under anticipated repository conditions.*

and it is predicted that all the O_2 in the repository environment will be consumed relatively early in the container lifetime (~2,600 years).[8] In the absence of significant O_2 concentrations, pitting of the canister surface should be severely restricted and the maximum depth of corrosion due to general corrosion and pitting is conservatively predicted to be 7.6 mm after 10^6 years.[7]

However, possible components of the immediate vault environment, as well as the bentonite clay, include pyrite (FeS_2) and sulfate (SO_4^{2-}), both of which are potential sources of sulfide, the latter (SO_4^{2-}) by reaction with sulfate-reducing bacteria (SRB), which can convert sulfates to sulfides.[9] Sulfate concentrations have been observed to increase substantially in bentonite pore water,[10] as a result of the dissolution of gypsum ($CaSO_4$).[1] Various factors, such as the mechanical pressure from the swelling bentonite, the low water activity in the bentonite, γ-radiation, and the heat from radionuclide decay processes should ensure that there is no microbial activity in the vicinity of the container.[9] The remotely produced sulfide, however, could be transported slowly through the compacted buffer to the container surface (Figure 2).[9] In the presence of sulfide, copper becomes a base metal, since its corrosion to produce extremely stable and insoluble sulfides, e.g.:[11-12]

$$2Cu + S^{2-} \rightarrow Cu_2S + 2e^- \quad (1)$$

can be sustained by the reduction of water:

$$2H_2O + 2e^- \rightarrow H_2 + 2OH^- \quad (2)$$

Whether or not this leads to extensive corrosion damage will be determined by the supply of sulfide and the protective properties of the sulfide film.

Swedish/Finnish studies have found proposed repository sites to contain significant amounts of sulfide, with predicted concentrations in the range of (0 to 3) × 10^{-3} mol/L at vault closure to (0 to 0.3) × 10^{-4} mol/L 10,000 years into the future.[13]

The possibility of sulfide-induced copper corrosion has been acknowledged in previous Swedish/Finnish models developed to predict the long-term corrosion of waste containers. To date, these models have been primarily based on thermodynamic principles. Assuming infinitely rapid interfacial kinetics, it was predicted that corrosion would be rate-controlled by the mass transport of sulfide to the container surface. Werme, et al.,[14] used a one-dimensional mass-transport-limited model to predict that sulfide concentrations in the repository bore holes will take approximately 850,000 years to be consumed. This is considerably longer than the ~1,000 years previously predicted.[15] Due to shallow concentration gradients, sulfide from sources external to the repository will not contribute to container corrosion during this time. This model predicts a maximum depth of corrosion due to direct sulfidation of ~1 mm over this time period.

The mixed potential model originally developed by King and Kolar[7] was subsequently extended to include the indirect effect of sulfide.[1] It was assumed that the corrosion rate will be sustained by any process capable of maintaining high concentration gradients of $CuCl_2^-$ at the container surface, thereby ensuring a rapid flux of soluble copper from the corroding surface. Sulfide has the potential to sustain this corrosion rate via a reaction with $CuCl_2^-$ to precipitate copper sulfides, a process that would increase the concentration gradient of Cu^I at the container surface, thereby sustaining the flux of Cu^I and, hence, the corrosion rate. The King and Kolar model predicts a maximum corrosion depth of <6 μm after 50,000 years, but does not take into account direct reaction of copper with sulfides and results in a corrosion rate ~5X less than that given by the model of Werme, et al., in 1992.[14]

The predominant focus of corrosion studies on copper materials in aqueous sulfide environments has been on the investigation of the behavior of Cu-Ni

alloys in polluted seawater with a primary emphasis on the effects of switching between anoxic and oxic conditions and the influence of sulfide on the formation of passive oxide films.[16-30] While these studies may be peripheral to our present interests, they clearly demonstrate the destabilization of passive oxide films in the presence of even small concentrations of sulfide.

Much less research has been carried out on the corrosion of unalloyed copper in sulfide-containing environments.[22-32] Mor and Beccaria[31] reported that the corrosion rate of copper increased with increasing pH and attributed this to the aggressive effect of S_2^-, despite the fact that the concentration of this ion was only in the range from 10^{-9} mol/L to 10^{-8} mol/L at the pH values used. In a study relevant to our present interests, King and Stroes-Gascoyne[11] measured corrosion potentials (E_{corr}) on a copper electrode covered with compacted clay under anoxic conditions. As observed by others in open solution,[17] the presence of sulfide caused a drop in E_{corr} to values close to the redox potential for the reaction:

$$2Cu + HS^- \leftrightarrow Cu_2S + H^+ + 2e^- \quad (3)$$

Subsequently, King[1] analyzed the available data on E_{corr} measurements on Cu in aqueous sulfide solutions and noted that, while the values were close to the equilibrium potential for Reaction (1), it was not possible to decide whether E_{corr} was a redox equilibrium potential or a mixed potential due to the coupling of the anodic reaction of Cu (the forward step in Reaction [1]) to the cathodic reduction of water.

The primary goals of the research described in the present paper are the following:

—to clarify the corrosion mechanism of copper in sulfide solutions
—to identify the nature of the phases formed
—to determine the current-potential relationships for the anodic and cathodic reactions involved in the corrosion process

These relationships will eventually form the basis of a mixed potential model for copper container corrosion under waste disposal conditions. Current experimental work has been performed under ambient conditions within a range of sulfide concentrations from 3×10^{-5} mol/L to 10^{-2} mol/L; however, future goals include the study of this system at temperatures of up to 80°C.

EXPERIMENTAL PROCEDURES

Materials and Electrode Preparation

All experiments were performed with phosphorous-doped, oxygen-free copper (Cu-OF) provided by the Swedish Nuclear Fuel and Waste Management Co. (SKB; Stockholm, Sweden). Working electrodes were prepared by machining copper discs of 1 cm diameter and threading them onto titanium rods. The copper discs were then either encased in polytetrafluoroethylene (PTFE) holders using epoxy resin (casting compound) or painted with lacquer to prevent any contact of the aqueous environment with the titanium contact. The copper discs were polished successively with 180-, 220-, 320-, 500-, 800-, 1,000-, and 1,200-grade silicon carbide (SiC) papers and then to a mirror finish using 1-μm, 3,000-Å, and 500-Å alumina-silicate suspensions. The discs were then washed with deionized Millipore† water (18.2 MΩ·cm), ultrasonically cleaned in a water bath, and given a final washing with deionized water prior to experiments.

Solutions

All solutions were prepared using ultrapure deionized water (18.2 MΩ·cm) and analytical-grade sodium chloride (NaCl, 99.0% assay) as a supporting electrolyte at a concentration of 0.1 mol/L. Sulfide solutions were prepared with reagent-grade sodium sulfide ($Na_2S \cdot 9H_2O$, 98.0% assay) in the total sulfide/bisulfide concentration ([S]T) range of 10^{-5} mol/L to 10^{-2} mol/L to simulate anticipated Scandinavian groundwater concentrations.

Electrochemical Cell and Equipment

All experiments were performed in a single compartment electrochemical cell with a fitted PTFE lid, using a copper disc working electrode, a platinum mesh counter electrode (9 cm^2), and a saturated calomel (SCE) reference electrode. All potentials are quoted against the SCE (–241 mV vs standard hydrogen electrode [SHE]). Rotating electrodes were controlled using a radiometer analytical rotator. Potentials were controlled using a Solartron 1287† potentiostat and electrochemical impedance spectroscopy was carried out using a Solartron 1254† frequency response analyzer. The software used for the analysis of the electrochemical impedance spectroscopy (EIS) data was Zview† version 2.80 produced by Scribner Associates Inc. (Southern Pines, North Carolina).

Experimental Procedure

To avoid contamination by atmospheric O_2, the majority of the experiments were performed in an anoxic chamber in Ar-purged solutions, and electrodes were cathodically cleaned at –1.3 V for 60 s and –1.15 V for 60 s prior to all experiments. This precaution was taken to avoid the oxidation of sulfide by dissolved oxygen, which has been shown to proceed through the sequence:

$$SH^- \rightarrow S_2^{2-} \rightarrow SO_3^{2-} \rightarrow SO_4^{2-} \rightarrow S_2O_3^{2-} \quad (4)$$

with oxidation to the oxyanions occurring only slowly.[33]

† Trade name.

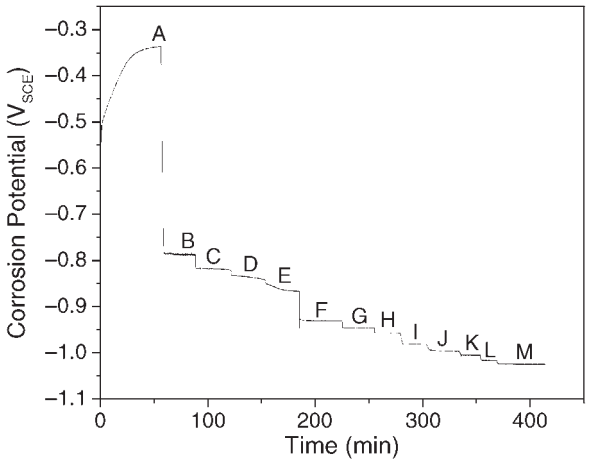

FIGURE 3. *E_{corr} as a function of total sulfide concentration (in mol/L) and time (stagnant solution): (A) 0.00, (B) 3.32 × 10^{-5}, (C) 6.62 × 10^{-5}, (D) 9.90 × 10, (E) 1.32 × 10^{-4}, (F) 4.59 × 10^{-4}, (G) 7.84 × 10^{-4}, (H) 1.11 × 10^{-3}, (I) 2.69 × 10^{-3}, (J) 4.23 × 10^{-3}, (K) 5.71 × 10^{-3}, (L) 8.55 × 10^{-3}, and (M) 1.12 × 10^{-2}.*

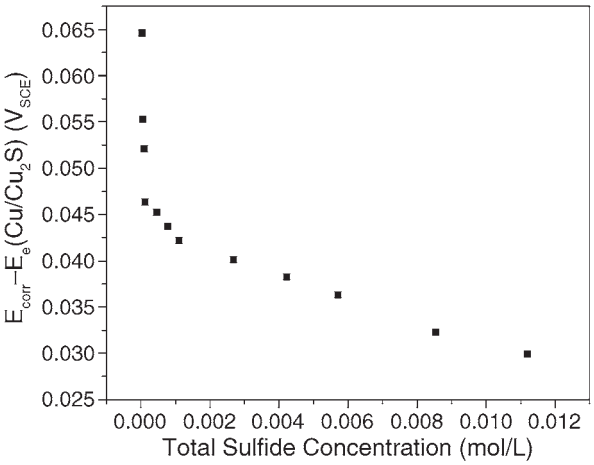

FIGURE 4. *The difference between the observed E_{corr} and the calculated reversible potential (E_e) for the Cu/Cu_2S reaction as a function of total sulfide concentration.*

Electrochemical experiments were performed either voltammetrically (2 mV/s) at rotating disc electrodes ($1 \le \omega \le 30$ Hz) or potentiostatically with intermittent EIS measurements. Also, E_{corr} measurements were made with intermittent EIS measurements. EIS spectra were recorded using a potential input signal of amplitude ±10 mV over the frequency range from 10^6 Hz to 10^{-2} Hz. On completion of the E_{corr} experiments, the extent of corrosion was determined by cathodically stripping the corrosion films using a potential scan from the measured corrosion potential to –1.6 V_{SCE}.

Analytical Methods

Scanning electron microscopy (SEM) was performed on samples corroded under open-circuit conditions in 0.1 mol/L NaCl solution containing a sulfide concentration of 10^{-3} mol/L for various lengths of time. On completion of the corrosion experiment, specimens were removed from solution and rinsed with deionized water (18.2 MΩ·cm) to remove NaCl prior to examination using an S-4500† scanning electron microscope.

Specimens for analysis by x-ray diffraction (XRD) were prepared in a similar manner and rinsed with deionized water (18.2 MΩ·cm) prior to analysis using a Bruker D8 Discover 2D GADDS† x-ray diffractometer.

RESULTS AND DISCUSSION

Corrosion Potential Studies

Figure 3 shows E_{corr} measured as a function of increasing sulfide concentration ($[S]_T$). The very negative E_{corr} value observed prior to the addition of sulfide is indicative of the anoxic conditions achieved within the anaerobic chamber. Comparison of this value to E/pH diagrams[34] clearly shows that, at this potential, copper is well below the threshold for copper oxide formation and is thermodynamically stable in water. However, the addition of even a small concentration of sulfide rapidly shifts E_{corr} to more negative values. Transition from E_{corr} value (A) to (B) requires approximately 1.5 min.

Figure 4 shows that E_{corr} approaches the equilibrium potential (E_e) for the Cu/Cu_2S reaction (Equation [3]) as $[S]_T$ is increased. In calculating $E_{corr} - E_e$, E_e is given by the Nernst relationship:

$$E_{e(Cu/Cu_2S)} = -1.13 - 0.030 \log[S^{2-}] \quad (5)$$

and the concentration of S_2^- at any given [S]T, and pH is determined from the dissociation equilibrium:

$$SH^- \leftrightarrow S^{2-} + H^+ \quad (6)$$

using a pKa value of 11.96.[32] However, some doubt exists, with values between 11.96 and 14.92 having been claimed.[12,31-34]

Considerable discussion has taken place about whether or not E_{corr} values for copper in aqueous sulfide solutions represent a redox potential for a reaction such as Reaction (3) or a mixed potential involving the coupling of the anodic part of Reaction (3) to the reduction of water.[25,31-32,35-36] Our observation, Figure 4, that E_{corr} approaches $E_{e\,(Cu/Cu_2S)}$ as the sulfide concentration is increased suggests that control of the potential by the Cu_2S redox reaction may be possible at high $[S]_T$. This would require that the sulfide film grows to an equilibrium state or constant thickness. The values of E_{corr} measured at lower $[S]_T$ (<4 × 10^{-3} mol/L) deviate significantly from $E_{e\,(Cu/Cu_2S)}$ and, from inspection of Figure 3, appear to be steady-state values; i.e., they do not slowly approach the redox potential. We conclude from this that, for the sulfide

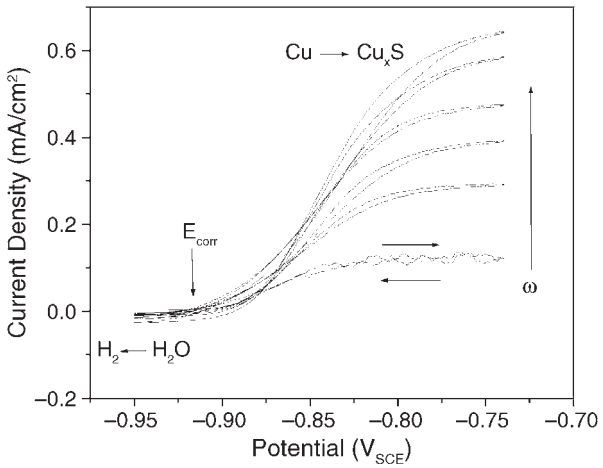

FIGURE 5. *Voltammetric scans recorded on a rotating disc electrode for $[S]_T = 10^{-3}$ mol/L at a scan rate of 2 mV/s and various electrode rotation rates (1, 6, 11, 16, 26, 30 Hz). These scans were performed from/to –1.35 V, but only the portion from/to –0.96 V is shown for clarity.*

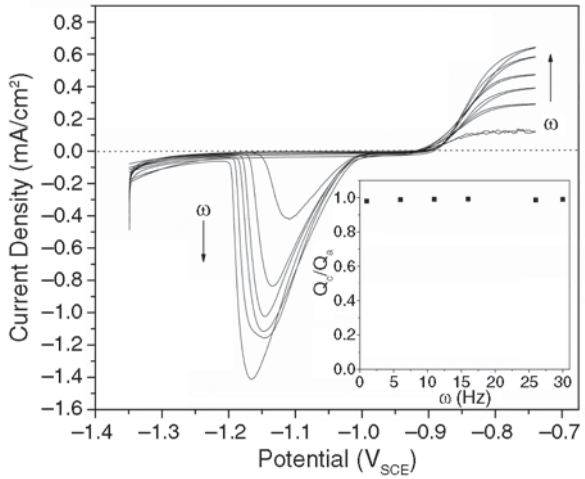

FIGURE 6. *Voltammetric scans recorded at rotating disc electrodes for $[S]_T = 10^{-3}$ mol/L (from Figure 5), showing the peaks associated with the cathodic reduction of the copper sulfide film. Inset shows cathodic (Q_C) to anodic (Q_A) charge ratios obtained by integration of the anodic and cathodic sections of the voltammogram.*

concentration range of primary interest (10^{-3} mol/L to 10^{-5} mol/L), E_{corr} is a mixed potential, with Reaction (3) potential-determining and the reduction of H_2O strongly polarized and rate-determining.

Cyclic Voltammetry at Rotating Disc Electrodes

Figure 5 shows anodic scans for cyclic voltammograms performed in a 10^{-3}-mol/L sulfide solution at various electrode rotation rates (ω). These scans were performed from/to a cathodic limit of –1.35 V, but only the portion of the scans from, and back to, –0.96 V is shown for clarity. As is clearest in the scan at ω = 6 Hz, anodic film growth occurs reversibly and under transport control. Extended versions of the voltammetric scans from –1.35 V to –0.75 V are plotted in Figure 6 to show the peaks associated with the cathodic reduction of the anodically grown copper sulfide film. The presence of a single reduction peak suggests only one phase is present. Integration of the anodic and cathodic currents for all the voltammograms shown in Figure 6 yields cathodic to anodic charge ratios of ~99.9% (Figure 6 inset), showing that regardless of rotation rate, all the charge injected on the anodic scan is available for reduction on the reverse cathodic scan. This indicates negligible dissolution, with all the charge associated with anodic film formation.

Also to be noted in Figures 5 and 6 are the very low currents in the potential range from –950 mV to –850 mV, an area where H_2O reduction currents are to be expected. The current in this region is independent of electrode rotation rate, sulfide concentration, and potential; i.e., the cathodic reduction of H_2O very rapidly becomes kinetically controlled. A possibility is that the currents in this region are due to the transport-limited reduction of traces of dissolved oxygen in solution. However, calculations show that for this

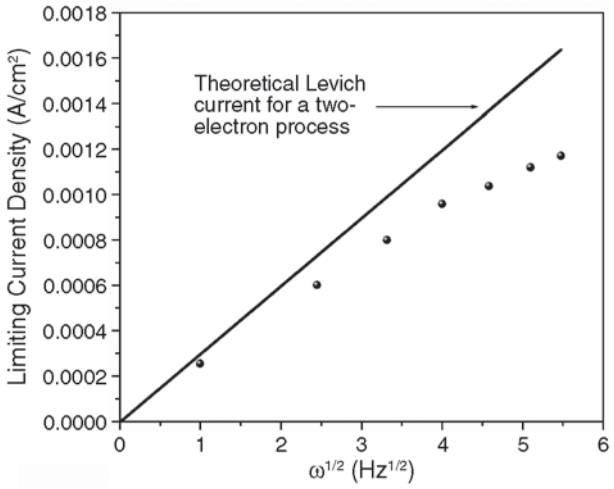

FIGURE 7. *Limiting anodic currents (from the voltammograms in Figure 5) as a function of the square root of electrode rotation rate (ω), showing that the limiting current approaches the theoretical Levich limiting current as ω → 0.*

to be the case would require a dissolved O_2 concentration of ~3.55×10^{-6} mol/L, a concentration well above that likely to persist in our prepurged solution introduced into an anoxic chamber. A more extensive series of rotating disc experiments are currently underway to elucidate more clearly the nature of this cathodic reaction.

The measured diffusion-limiting anodic currents in the voltammograms of Figures 5 and 6 approach the theoretical Levich limiting currents as the electrode rotation rate tends to zero (Figure 7). The deviation of the limiting current from the predicted values as ω increases suggests a limitation on the anodic film formation rate due to the presence of a surface film.

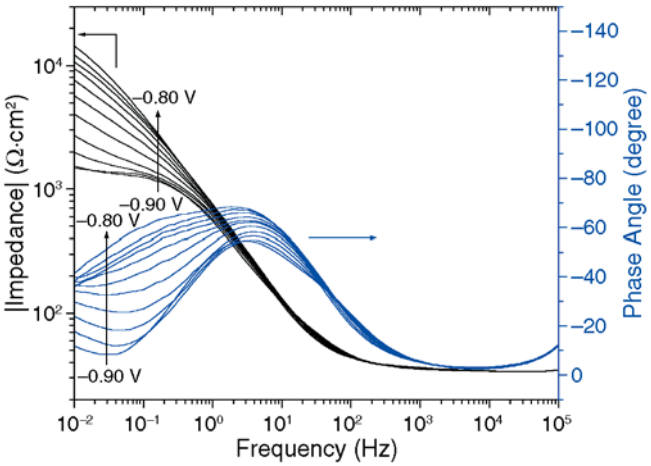

FIGURE 8. *EIS data (phase angle [θ] and absolute impedance [Z] vs. frequency) as a function of anodic potential, $[S]_T = 10^{-3}$ mol/L: –0.90 V, –0.89 V, –0.88 V, –0.87 V, –0.86 V, –0.85 V, –0.84 V, –0.83 V, –0.82 V, –0.81 V, and –0.80 V.*

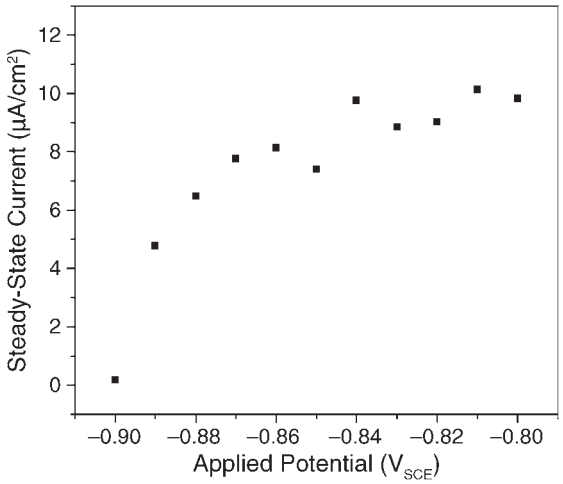

FIGURE 9. *Plot showing the steady-state current density as a function of applied potential prior to the measurement of the spectra in Figure 8.*

Electrochemical Impedance Spectroscopy

Figure 8 shows EIS data recorded under potentiostatic conditions. Each spectrum was recorded after the electrodes reached a steady-state current (2 h) at a potential in the range from –0.90 V to –0.80 V. In these experiments the electrode was not rotated. This data proved difficult to accurately fit to a specific equivalent circuit, but a number of features can be noted. The time constant at the highest frequency (in the range from 5 Hz to 10 Hz) shows little change with increasing potential. This time constant is consistent with a potential-independent interfacial charge transfer to produce Cu^{I} controlled by SH^- transport. A second time constant appears with increasing potential in the 10^{-1}-Hz range, leading to an increase in overall impedance, consistent with the growth of a surface film. Also, with the increase in applied potential, the phase angle approaches 45°, the value expected for a totally diffusion-controlled process. This suggests that while a surface film may be present, the electrochemical current becomes more transport-controlled as potential increases. This is consistent with the observed decrease in dependence of the steady-state current density on applied potential (Figure 9) and with the large Warburg impedance values coupled with relatively small total resistances obtained when trying to fit the impedance spectra.

Figure 10 shows EIS measurements recorded in a 10^{-3}-mol/L $[S]_{total}$ solution under natural corrosion conditions. The system rapidly attains a steady-state and remains stable over the 46-h duration of the experiment. This is also reflected in the corresponding E_{corr} values, which quickly relax from ~–0.94 V to a steady-state value of ~–0.96 V as a coherent Cu_xS film forms, Figure 11. The E_{corr} measurements shown in Figure 11 were recorded consecutively, interrupted by 2-h EIS experiments. The value for the phase angle (θ) at frequencies less than 10 Hz and the reduced slope of the log |Z| vs. log frequency plot as frequency tends to 0 Hz indicate that the impedance behavior cannot be represented by a simple parallel RC circuit and can only be fitted using a circuit that incorporates a Warburg coefficient for diffusion effects (Figure 10 [inset]). In this circuit, R_1 is the polarization resistance, C_1 is the interfacial capacitance, and W is the Warburg impedance for diffusive transport.

A good fit to the data was obtained and Figure 12 shows the total surface capacitance (C_1) given by:

$$(C_1)^{-1} = C_{dl}^{-1} + C_F^{-1} \quad (7)$$

where C_F is the film capacitance and C_{dl} is the capacitance of the double layer. The polarization resistance (R_1) is a function of the duration of exposure to the sulfide solution. Values of the Warburg impedance were also obtained but were very unreliable because of the large error involved in extrapolating the low-frequency data to obtain the values. However, W is orders of magnitude greater than R_1, indicating control of the corrosion process by solution transport of SH^- under the stagnant conditions used. This is consistent with the data in Figure 7, which shows that sulfide film formation becomes transport-limited as $\omega \rightarrow 0$. Estimates of diffusion layer thickness (assuming a commonly observed value for the SH^- diffusion coefficient of 10^{-5} cm^2/s) yield values in the range of 0.5 mm to 2 mm, which are not unreasonable for stagnant solutions.

The very small values of R_1 indicate the surface sulfide film does not significantly impede the corrosion process. The increase of R_1 with time (Figure 12) would be consistent with the minor thickening of the film suggested by the slight decrease in C_1 over the same period, if we assume the double-layer capaci-

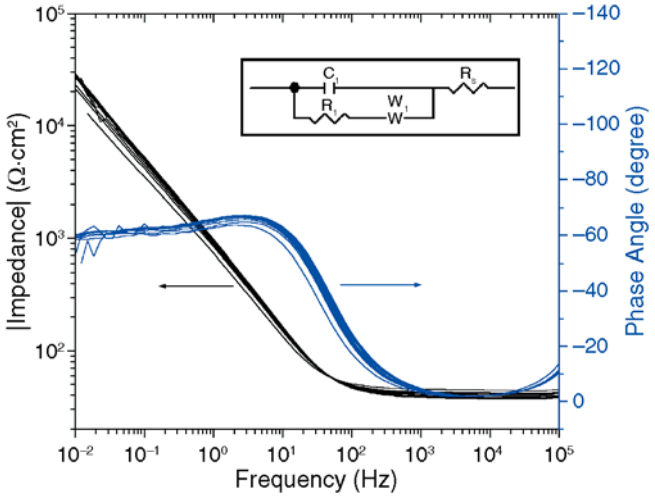

FIGURE 10. *EIS data recorded during corrosion in a solution containing 10^{-3} mol/L sulfide. This plot includes 10 spectra recorded over the 46-h duration of the experiment. The inset shows the equivalent circuit used to fit the data.*

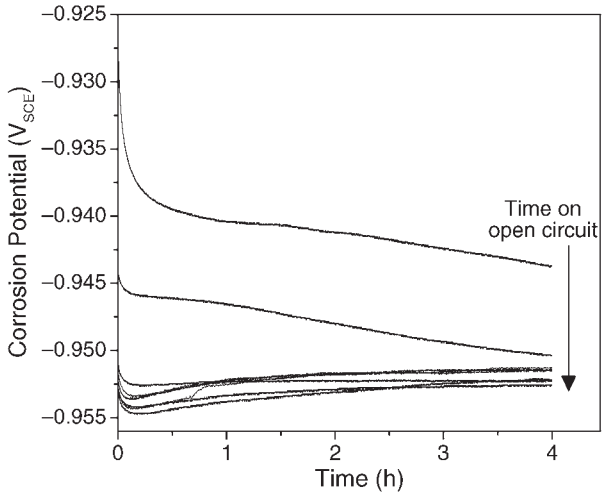

FIGURE 11. *E_{corr} for corrosion in stagnant solution conditions containing 10^{-3} mol/L sulfide.*

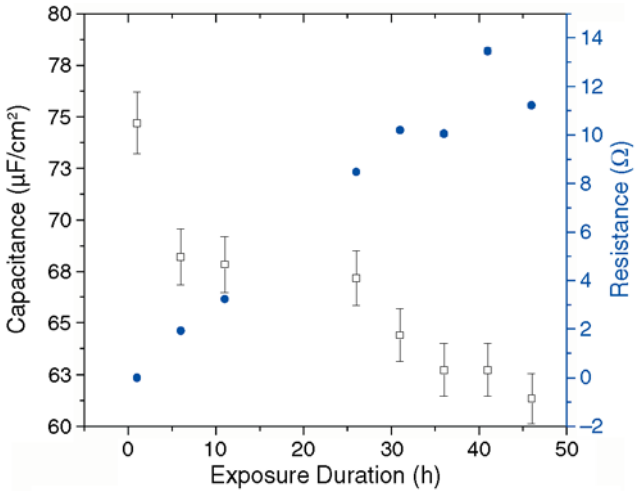

FIGURE 12. *Total capacitance (C_1) and resistance (R_1) as a function of exposure duration for a copper electrode in 10^{-3} mol/L sulfide solution. Values were obtained from a fit to the equivalent circuit shown in Figure 10.*

tance remains constant and attribute the change in C_1 completely to the thickening of the film. The fact that the capacitance changes little after the first 10 h, the period over which E_{corr} changes before establishing an approximate steady-state value, suggests rapid film formation at short exposure times with a slow to negligible growth thereafter.

To obtain a reliable measure of film thickness from these capacitance values we would need to know both the double-layer capacitance and a value for the dielectric constant of the sulfide film. Assuming a value of C_{dl} = 20 μF/cm² and taking the dielectric constant to be in the range from 20 to 80 yields film thicknesses in the region from 100 nm to 650 nm. A higher assumed value of C_{dl} would yield smaller film thicknesses.

Cathodic Stripping Voltammetry

In a second series of corrosion experiments, the sulfide films were cathodically stripped after various periods of exposure. The E_{corr} values in these experiments agreed closely with those measured in the impedance experiments described above, making the two sets of data comparable. Figures 13 and 14 show that the cathodic stripping voltammograms (CSVs), recorded after corrosion, fall into two categories: those that exhibit a small reduction charge generally associated with a single reduction peak (Figure 13) and those that exhibit a significantly greater reduction charge often associated with two reduction peaks (Figure 14). For this second category, the first reduction peak occurs in the same potential range as the smaller peak in Figure 13, while the second larger reduction peak occurs at significantly more negative potentials. No apparent correlation between the E_{corr} value measured and either of these two behaviors is observed.

These observations indicate two distinct film growth patterns, a suggestion supported by the charge time plots (Figure 15) obtained by integrating the charge under the film reduction peaks in Figures 13 and 14. Initial film growth would be expected to occur by ionic or defect transport through the growing sulfide film. A significant ionic conductivity in the solid state is expected for compounds containing large anions (S^{2-}) and relatively small cations (Cu^{+}) with the latter, or an associated defect, being the mobile species.[37-38] Along this pathway, the film would be expected to approach a limiting thickness as suggested by line 1 in Figure 15. This would be consistent with the impedance data described in Figures 10 through 12, which shows that the corrosion process leading to the formation of this film is rapid.

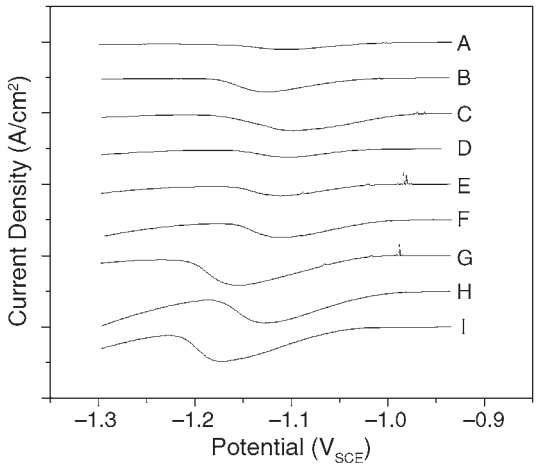

FIGURE 13. *Cathodic stripping voltammograms recorded after various periods of exposure to a sulfide solution (10^{-3} mol/L): (A) 0.5 h, (B) 1 h, (C) 2 h, (D) 4 h, (E) 7 h, (F) 14 h, (G) 20 h, (H) 24 h, and (I) 34 h. The current densities have been offset for clarity.*

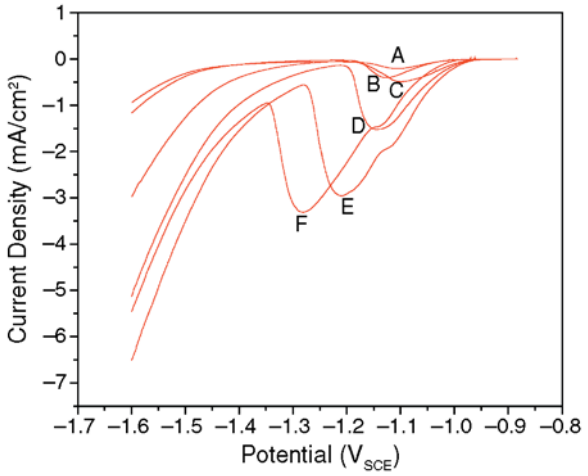

FIGURE 14. *Cathodic stripping voltammograms recorded after various periods of exposure to a sulfide solution (10^{-3} mol/L): (A) 0.5 h, (B) 1 h, (C) 4 h, (D) 20 h, (E) 44 h, and (F) 48 h.*

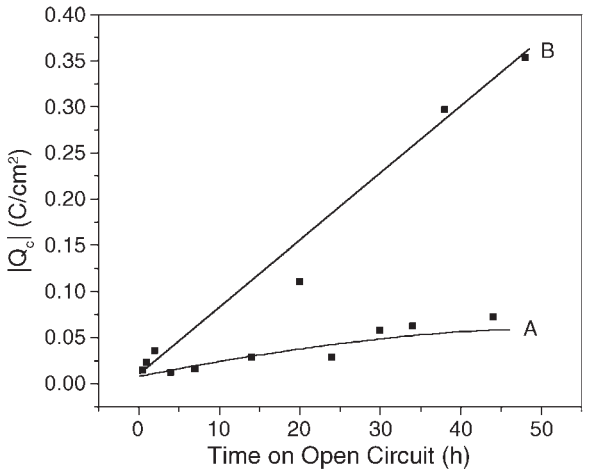

FIGURE 15. *Plot of cathodic charge (Q_C) as function of exposure to a sulfide solution (10^{-3} mol/L) (obtained by integration of the cathodic peaks in Figures 13 and 14).*

However, because of the large size of the anion (S^{2-}), this film would have a large Pilling-Bedworth ratio, which could lead to compressive interfacial stresses and film fracture. Subsequently, growth would occur by transport through fractures (or pores), a process that would bypass the growth limitations imposed by solid-state transport and allow film growth to proceed to substantially greater thicknesses (line 2 in Figure 15). This second process would lead to the observation of the dual film reduction process observed in Figure 14, which corresponds to a first small reduction peak at a less negative potential due to the reduction of the initially formed layer and a second peak at a more negative potential due to the reduction of the thicker outer layer film (Figure 14). It would be expected that, for natural corrosion conditions, this second pathway would be more prominent than the first.

The ongoing growth of this second thicker, outer layer could be sustained by the formation of soluble complexes such as CuHS (aq), $Cu(HS)_2^-$, and $Cu_2S(HS)_2^{2-}$ in the concentrated solutions formed within the pores. Thermodynamic evidence exists demonstrating the influence of such complexes on the solubility of copper sulfides,[4,39-40] and it has been suggested[4] that such complexes may be responsible for Cu migration and mineralization in natural reducing sulfide environments. Dual layer growth has been claimed for the formation of copper sulfide films on Cu-Ni alloys,[28] supported by SEM evidence showing the presence of a porous film, and for the electrochemical growth of sulfide films on Cu based on the form of potentiostatically recorded current-time plots.[32,41]

Thermodynamic calculations[40] and E-pH diagrams[4] show that stability fields exist for a range of copper sulfides; namely, chalcocite (Cu_2S), djurleite ($Cu_{1.934}S$), digenite ($Cu_{1.8}S$), anilite ($Cu_{1.75}S$), and, for slightly more oxidizing conditions, covellite (CuS). Of these phases, the stability field for chalcocite extends beyond (i.e., to lower potentials than) the stability field for water for $[S]_T$ as low as 10^{-5} mol/L, making this the most stable phase under the conditions of our experiment.

Surface Analysis

To determine the phase(s) formed, XRD analysis of corrosion products was performed on samples corroded under open-circuit conditions in a 10^{-3}-mol/L sulfide solution. Samples were removed from solution after 1 h, 8 h, 24 h, and ~9 days. E_{corr} values measured in these preparations agreed well with those observed in all previous experiments discussed. XRD

results reveal the corrosion product after 1 h to be comprised of a main phase of Cu_2S (chalcocite) and a minor phase of $Cu_{1.8}S$ (digenite). These two copper sulfides are present in the corrosion product of every sample, with chalcocite being the dominant phase in all experiments. It is also evident that the corrosion product continues to thicken with exposure to solution in these experiments, i.e., appears to follow reaction path 2 (Figure 15). A diminishing dominance of the Cu substrate peaks was observed as the time in solution increased. These two phases were also observed on Cu-Ni alloys after corrosion in aqueous sulfide.[25] No covellite (CuS), claimed as the product of anodic oxidation,[32,41] was observed, which is consistent with thermodynamic expectations for corrosion at potentials below the stability line for water.

Scanning electron micrographs of corrosion products were also obtained. Again, samples were prepared under open-circuit conditions in an anoxic 10^{-3}-mol/L solution and removed after 1 h, 8 h, and 24 h. The E_{corr} values were consistent with those observed previously. SEM shows the surface to be covered by a nodular deposit (Figures 16[a] through [d]), suggesting that growth of the outer layer occurs by a nucleation and growth process. Surface features remain approximately the same size regardless of the duration of corrosion. It appears that the film becomes much thicker with time in solution. At the end of 24 h, an extremely flawed and porous, sponge-like deposit can be seen (Figures 16[c] and [d]), indicating the on-going accumulation of a thick outer layer of deposit. These observations are also consistent with an on-going film growth process following pathway 2 in Figure 15.

CONCLUSIONS

❖ In anoxic aqueous conditions containing dissolved sulfide, copper is thermodynamically unstable and the anoxic growth of a copper sulfide film is supported by the cathodic reduction of water.
❖ XRD shows that this film is predominantly chalcocite (Cu_2S) with some digenite ($Cu_{1.8}S$).
❖ On a clean copper surface, film growth occurs rapidly and is controlled by the diffusive transport of SH^- to the electrode surface under stagnant conditions.
❖ At a sulfide concentration of 10^{-3} mol/L, film growth can follow two distinct pathways. The initially formed film grows via the transport of Cu^I ions (or an associated defect) through the sulfide film. If this film remains intact, then film growth is limited and a steady-state thickness is achieved. If the development of interfacial stresses leads to film fracture, then growth can continue and much thicker nodular deposits, confirmed using SEM, are formed.
❖ When an intact sulfide film is present the corrosion potential achieves a value very close to the equilibrium potential for the sulfide formation reaction. This, and the observation that the cathodic current for H_2O reduction is very small and potential independent, shows that the sulfide formation reaction is rate-determining.
❖ While these studies provide a preliminary understanding of the mechanism of copper corrosion in the presence of sulfide, considerable additional effort is required before the kinetic basis for a mixed potential model can be specified.

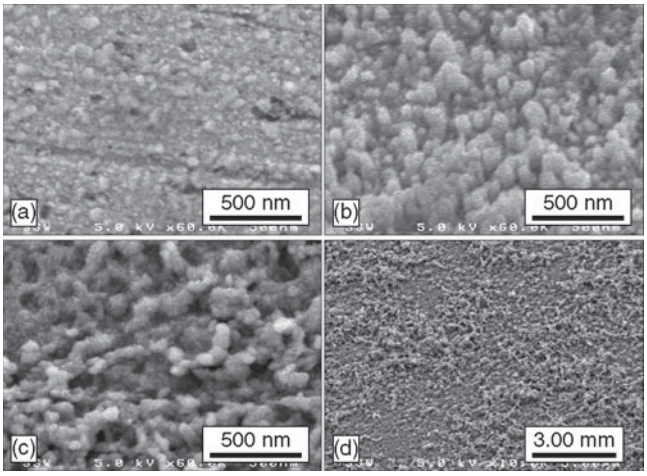

FIGURE 16. *Scanning electron micrographs of copper sulfide films formed by corrosion in a 10^{-3}-mol/L sulfide solution for a duration of: (a) 1 h, (b) 8 h, and (c,d) 24 h.*

ACKNOWLEDGMENTS

This research has been funded by the Swedish Nuclear Fuel and Waste Management Co. (SKB), Stockholm. In addition, the authors would like to thank R. Flemming and T. Karamaneva of the Department of Earth Sciences in the University of Western Ontario (London, Ontario, Canada) for the XRD analyses and Surface Science Western (London, Ontario, Canada) for the use of their scanning electron microscope.

REFERENCES

1. F. King, "Corrosion of Copper in Alkaline Chloride Environments," Swedish Nuclear Fuel and Waste Management Co. Technical Report, TR-02-25, 2002.
2. J. McMurry, "Evolution of a Canadian Deep Geologic Repository: Base Scenario," Ontario Power Generation Report no. 06819-REP-01200-10092-R00, 2003.
3. J. McMurry, "Evolution of a Canadian Deep Geologic Repository: Base Scenario," Ontario Power Generation Report no. 06819-REP-01200-10127-R00, 2004.
4. I. Puigdomenech, "Thermodynamic Data for Copper. Implications for the Corrosion of Copper Under Repository Conditions," C. Taxen, SKB Swedish Nuclear Fuel and Waste Management Co. Technical Report, TR-00-13, 2000.
5. C. Andersson, "Development of Fabrication Technology for Copper Canisters with Cast Inserts. Status Report in August 2001," SKB Swedish Nuclear Fuel and Waste Management Co. Technical Report, TR-02-07, 2002.
6. P Maake, "Used Fuel Container Requirements," Ontario Power Generation Report no. 06819-PDR-01110-R01, 2001.

7. F. King, M. Kolar, Ontario Power Generation, Nuclear Waste Management Division Report, 06819-REP-01200-10041-R00 (2000).
8. F. King, "Mechanistic Modeling of the Corrosion Behavior of Copper Nuclear Fuel Waste Containers," Proc. Int. Conf. on Deep Geological Disposal of Radioactive Waste (Toronto, ON, Canada: Canadian Nuclear Society, 1996), p. 5-39.
9. K. Pederson, "Microbial Processes in Radioactive Waste Disposal," SKB Swedish Nuclear Fuel and Waste Management Co. Technical Report, TR-00-04, 2000.
10. A. Muurinen, J. Lehikoinen, "Porewater Chemistry in Natural Bentonite," Posiva Oy, Report 99-20, 1999.
11. F. King, S. Stroes-Gascoyne, "Microbially Influenced Corrosion of Nuclear Fuel Waste Disposal Containers," Proc. 1995 Int. Conf. on MIC (Houston, TX: NACE International; Miami, FL: American Welding Society, 1995), p. 35/1-35/14.
12. M. Pourbaix, A. Pourbaix, Geochim. Cosmochim. Acta 56 (1992): p. 3,157.
13. P. Pitkanen, A. Luukkonen, P. Ruotsalainen, H. Leino-Forsman, U. Vuorinen, "Geochemical Modeling of Groundwater Evolution and Residence Time at the Olkiluoto Site," Posiva Oy, Report 98-10, 1999.
14. L. Werme, P. Sellin, N. Kjellbert, "Copper Canisters for Nuclear High Level Waste Disposal: Corrosion Aspects," SKB Swedish Nuclear Waste Management Co. Technical Report, TR-92-26, 1992.
15. "Final Storage of Spent Nuclear Fuel," SKB Swedish Nuclear Waste Management Co. Report, KBS-3, 1983.
16. P.A. Akolzin, A.F. Bogachev, Prot. Met. 5 (1969): p. 262.
17. H. Yamada, T. Nakamura, J. Jpn. Foundrymen's Soc. 36 (1964): p. 470.
18. J.C. Rowlands, J. Appl. Chem. 15 (1965): p. 57.
19. E.D. Mor, A.M. Beccaria, Corrosion 30 (1974): p. 354.
20. J.F. Bates, J.M. Popplewill, Corrosion 31 (1975): p. 269.
21. J.P. Gudas, H.P. Hack, Corrosion 35 (1979): p. 259.
22. B.C. Syrett, Corrosion 33 (1977): p. 257.
23. L. Giuliani, G. Bombara, Br. Corros. J. 8 (1973): p. 20.
24. H.P. Hack, J.P. Gudas, Corrosion 35 (1979): p. 67.
25. D.D. MacDonald, B.C. Syrett, S.S. Wing, Corrosion 35 (1979): p. 367.
26. B.C. Syrett, Corros. Sci. 21 (1981): p. 187.
27. L.E. Eiselstein, B.C. Syrett, S.S. Wing, R.D. Caligiuri, Corros. Sci. 23 (1983): p. 223.
28. D.D. MacDonald, B.C. Syrett, S.S. Wing, Corrosion 34 (1978): p. 289.
29. B.C. Syrett, D.D. MacDonald, Corrosion 35 (1979): p. 505.
30. B.C. Syrett, S.S. Wing, Corrosion 36 (1980): p. 73.
31. E.D. Mor, A.M. Beccaria, Br. Corros. J. 10 (1975): p. 33.
32. M.R. Gennero de Chialvo, A.J. Arvia, J. Appl. Electrochem. 15 (1985): p. 685.
33. M. Avrahami, R.M. Golding, J. Chem. Soc. A 3 (1968): p. 647.
34. M. Pourbaix, Atlas of Electrochemical Equilibria in Aqueous Solutions, 2nd ed. (Houston, TX: NACE International, 1974), p. 551.
35. F. King, C.D. Litke, M.J. Quinn, D.M. LeNeveu, Corros. Sci. 37 (1995): p. 833.
36. I.S. Escobar, E. Silva, C. Silva, A. Ubal, "Study of the Effect of Sulfide Ions on the Corrosion Resistance of Copper for Use in Containers for High-Level Waste," Proc. 4th Int. Conf. Copper 99-Cobre 99, vol. 1 (1999), p. 371.
37. R.V. Bucur, R. Berger, Solid State Ion. Diffus. React. 76 (1995): p. 291.
38. R. Berger, R.V. Bucur, Solid State Ionics 89 (1996): p. 269.
39. D.A. Crerar, N.L. Barnes, Econ. Geol. 71 (1976): p. 772.
40. B.W. Mountain, T.M. Seward, Geochim. Cosmochim. Acta 63 (1999): p. 11.
41. D. Vasquez Moll, M.R.G. de Chialvo, R.C. Salvarezza, A.J. Arvia, Electrochim. Acta 30 (1985): p. 1,011.